



A Journal of the Gesellschaft Deutscher Chemiker

# Angewandte Chemie

GDCh

International Edition

www.angewandte.org

## Accepted Article

**Title:** Bright and Stable NIR-II J-aggregated AIE Dibodipy for Dynamic in vivo Bioimaging

**Authors:** Fan Zhang, Qisong Zhang, Peng Yu, Yong Fan, Caixia Sun, Haisheng He, Xuan Liu, Lingfei Lu, Mengyao Zhao, and Hongxin Zhang

This manuscript has been accepted after peer review and appears as an Accepted Article online prior to editing, proofing, and formal publication of the final Version of Record (VoR). This work is currently citable by using the Digital Object Identifier (DOI) given below. The VoR will be published online in Early View as soon as possible and may be different to this Accepted Article as a result of editing. Readers should obtain the VoR from the journal website shown below when it is published to ensure accuracy of information. The authors are responsible for the content of this Accepted Article.

**To be cited as:** *Angew. Chem. Int. Ed.* 10.1002/anie.202012427

**Link to VoR:** <https://doi.org/10.1002/anie.202012427>

## COMMUNICATION

Bright and Stable NIR-II J-aggregated AIE Dibodipy for Dynamic *in vivo* Bioimaging

Qisong Zhang, Peng Yu, Yong Fan\*, Caixia Sun, Haisheng He, Xuan Liu, Lingfei Lu, Mengyao Zhao, Hongxin Zhang, Fan Zhang\*

**Abstract:** Organic dyes, emitting in the second near-infrared (NIR-II, 900-1700 nm) window, with high molar extinction coefficient (MEC) and quantum yield (QY) in aqueous is essential for *in vivo* bioimaging and biosensing. In this work, we developed a dibodipy based J-aggregated aggregation induced emission (AIE) molecule **THPP** to meet this aim. **THPP** exhibits a high MEC of dibodipy structure and has intensified absorption and emission in J-aggregated state, which significantly enhanced the fluorescence intensity (~55 folds) and extends the maximal absorption/emission wavelengths to 970/1010 nm in NIR-II region. Based on the bright **THPP**, imaging with high frame rate (34 frames per second) in a deep 'valid penetration depth' up to 6 mm can be achieved. This enabled simultaneously and dynamically imaging of vasculatures and deeply located visceral. Besides, we succeeded in monitoring the respiratory rate of acute-lung-injury mice and tracing the collateral circulation process with a high frame rate.

Fluorescence imaging is of paramount importance in the medical diagnosis,<sup>[1]</sup> drug delivery<sup>[2]</sup> and image-guided surgery,<sup>[3]</sup> especially in the state-of-the-art second near-infrared (NIR-II, 900-1700 nm) window,<sup>[4]</sup> where photons are rarely scattered and tissue autofluorescence is also diminished, therefore imaging with high signal-to-noise ratio (SNR) and high spatio-temporal resolution can be achieved in deep tissue.<sup>[5]</sup> Compared to inorganic probes, the NIR-II small organic molecules with good biocompatibility<sup>[6]</sup> have been used to improve imaging quality at superficial vasculature.<sup>[7]</sup> However, the limitation of the organic probes up to now is still the low fluorescence brightness in the NIR-II region, thus imaging deeply located viscera has rarely been reported. The dominating factors that affect the fluorescence brightness of fluorescent dyes are molar extinction coefficient (MEC) and quantum yield (QY). In recent studies, attention has been given to the donor-acceptor-donor (D-A-D) structure molecules and cyanines.<sup>[8]</sup> Cyanines show a high MEC ( $\sim 10^5 \text{ M}^{-1}\text{cm}^{-1}$ ) in organic solution, but the characteristics of seriously attenuation in aqueous ( $\sim 10^4 \text{ M}^{-1}\text{cm}^{-1}$ , e.g. IR26) and the aggregation caused quenching effect (ACQ) limited the actual applications.<sup>[9]</sup> To address the ubiquitous ACQ effect of organic dyes, great efforts have been made by introducing aggregation induced emission (AIE) function groups.<sup>[10]</sup> Owing to the AIE groups, D-A-D molecules show a higher QY in aggregation state,<sup>[11]</sup> but the inherent low MEC feature of D-A-D molecule ( $\sim 10^4 \text{ M}^{-1}\text{cm}^{-1}$ ) could hardly be improved by simple modification of the molecule.<sup>[12]</sup> In the meantime, aggregation usually causes wavelength shift, in which the bathochromic shift (J-aggregation) is of great value for *in vivo* imaging. However, it's still a big

challenge to realize both NIR-II AIE with high MEC and J-aggregation essence for dyes.<sup>[13]</sup>

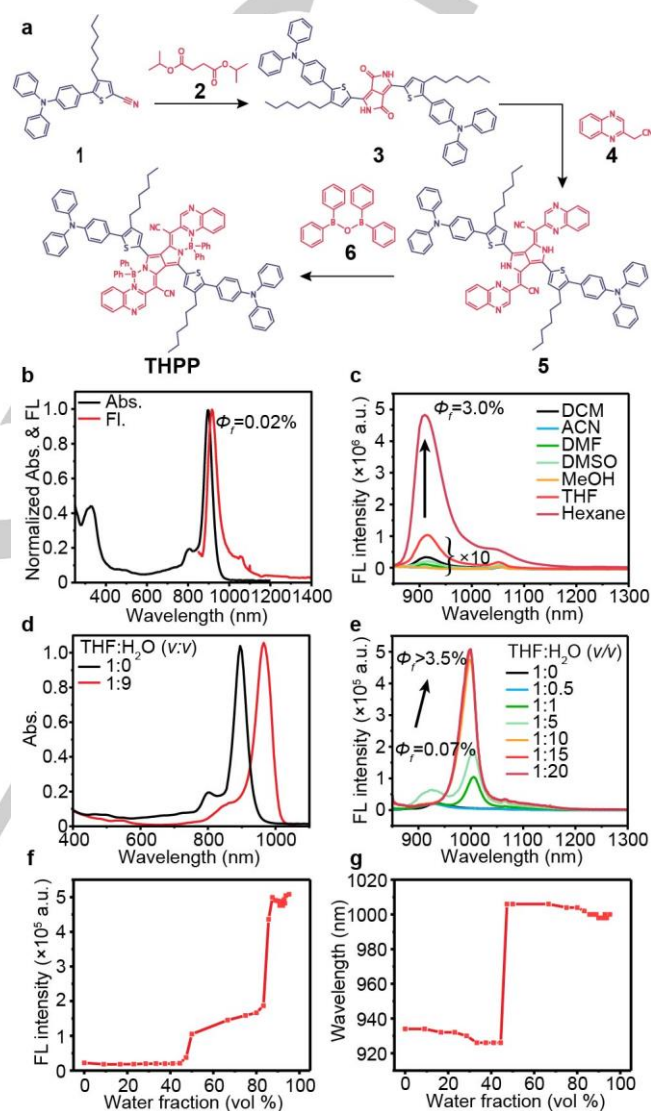


**Figure 1.** a) Scheme for the simplified synthetic route of **THPP**. b) Normalized absorption and emission spectra of **THPP** in dichloromethane. c) Emission spectra of **THPP** in different organic solution. d) Absorption spectra of **THPP** (5  $\mu\text{M}$ ) in THF and THF:H<sub>2</sub>O = 1:9 (v/v) solution. e) Fluorescence spectra of **THPP** in different ratio of THF:H<sub>2</sub>O mixed solution. f,g) Fluorescence intensity and wavelength of **THPP** as a function of water fraction. All the emission spectra were collected with an 808 nm laser at power density of  $0.5 \text{ W cm}^{-2}$ . Abs.: absorbance, FL: fluorescence.

Q. Zhang, P. Yu, C. Sun, Prof. Y. Fan, H. He, X. Liu, M. Zhao and Prof. F. Zhang  
 Department of Chemistry, State Key Laboratory of Molecular Engineering of Polymers and iChem, Shanghai Key Laboratory of Molecular Catalysis and Innovative Material, Fudan University, Shanghai 200433, China  
 E-mail: fan\_yong@fudan.edu.cn and zhang\_fan@fudan.edu.cn  
 Supporting information for this article is given via a link at the end of the document.

Herein, we report a bright ( $\epsilon\Phi_f > 7700 \text{ M}^{-1}\text{cm}^{-1}$ ) and stable AIE dibodipy **THPP** with J-aggregated characteristics in aggregated state to generate bathochromic shift with maximal absorption/emission wavelengths extended to 970/1010 nm in

## COMMUNICATION

aqueous. The enhanced fluorescence brightness is ascribed to the enhanced absorptivity ( $\epsilon$  is from  $2 \times 10^5 \text{ M}^{-1} \text{ cm}^{-1}$  to  $2.4 \times 10^5 \text{ M}^{-1} \text{ cm}^{-1}$ ) and QY ( $\Phi_f$  is from 0.07% to above 3.5%) in J-aggregated state. Due to the rigid planar structure, **THPP** shows an excellent performance in photostability and chemical stability. Based on the bright **THPP**, we could image cerebral and body vessels, as well as locate the deep visceral (heart, lungs, kidneys and spine) of mice with high SNRs dynamically. In addition, respiratory rate from mice with acute-lung-injury and monitoring the collateral circulation process can also be achieved using **THPP** with a imaging frame rate, suggesting the potential of **THPP** for high spatio-temporal *in vivo* imaging.

The simplified synthesis procedure of **THPP** is illustrated in Figure 1a. Compound 1 was synthesized from commercially available 2-bromo-3-hexylthiophene by Vilsmeier-Haack reaction, cyanation and Suzuki coupling with (4-(diphenylamino)phenyl)boronic acid (Scheme S1). Followed by the classic cyclization with succinate (compound 2), compound 1 turns into the dark blue DPP (diketopyrrolopyrrole, compound 3). After a phosphorous oxychloride activated condensation reaction with 2-(quinoxalin-2-yl)acetonitrile (compound 4), key intermediate compound 5 was synthesized. Finally, a coordination reaction with 1,1,3,3-tetraphenyldiboroxane (compound 6) affords **THPP** by yield of 19% (design stratagem as shown in Scheme S1, and complete synthesis procedure is shown in Scheme S2).

The maximum absorption and emission wavelength of **THPP** in DCM were 900/920 nm (Figure 1b). Benefits from the extended dibodipy structure, **THPP** shows a high MEC ( $\epsilon = 2 \times 10^5 \text{ M}^{-1} \text{ cm}^{-1}$ ), which is roughly an order of magnitude higher than that of the conventional D-A-D molecules ( $\sim 10^4 \text{ M}^{-1} \text{ cm}^{-1}$ ).<sup>[10g]</sup> In the polar solvent (such as DCM, THF and so on), monodispersed **THPP** molecule was suffered from twisted intramolecular charge transfer (TICT) effect of the free rotated triphenylamine (TPA) group,<sup>[14]</sup> which leads to low QYs of 0.02% and 0.07% in DCM and THF, respectively (using IR26 as a reference,  $\Phi_f = 0.05\%$ , Table 1). Nevertheless, when **THPP** was dissolved into apolar solvent (such as hexane and glyceride), the TICT effect was immediately restricted and the QYs were enhanced by 150 folds ( $\Phi_f = 3.0\%$ , Figure 1c and Table 1).

The above results showed a typical TICT characteristic of **THPP**. To further investigate the optical properties of **THPP**, measurement were conducted in the mixed solution of THF and H<sub>2</sub>O. **THPP** shows a bathochromic shift ( $\Delta\lambda = 80 \text{ nm}$ ) with an absorption and QYs increase when THF:H<sub>2</sub>O is 1:9 (Figure 1d and Table 1). With water fraction increased (from 0 to 50%), the emission intensity of **THPP** at 932 nm was slightly decreased at the initial stage, and then the spectra exhibited a bathochromic shift from 932 to 1010 nm, followed by a skyrocketing of fluorescence intensity (Figure 1e,f and S1). Meanwhile, the full width at half maxima (FWHM) of emission spectra gradually narrow down from 65 nm to 36 nm, confirming the AIE characteristic, which enhanced the intensity ( $\epsilon\Phi_f > 7700 \text{ M}^{-1} \text{ cm}^{-1}$ ) over 55 folds than that in bare THF ( $\epsilon\Phi_f = 140 \text{ M}^{-1} \text{ cm}^{-1}$ ). By further considering the gradually disappeared emission at 800 nm, the above characteristics are also pointing to the typical characterization of J-aggregation in this mixed solution.<sup>[15]</sup> Moreover, it can be confirmed that the rigid planar core structure of dibodipy ensures **THPP** a high MEC and the appended TPA

group affords a typical AIE performance. Taking advantages of all these outstanding performance, strong fluorescence with longer emission wavelength in the NIR-II region was realized by **THPP**, which is particularly important for dynamic *in vivo* bioimaging.

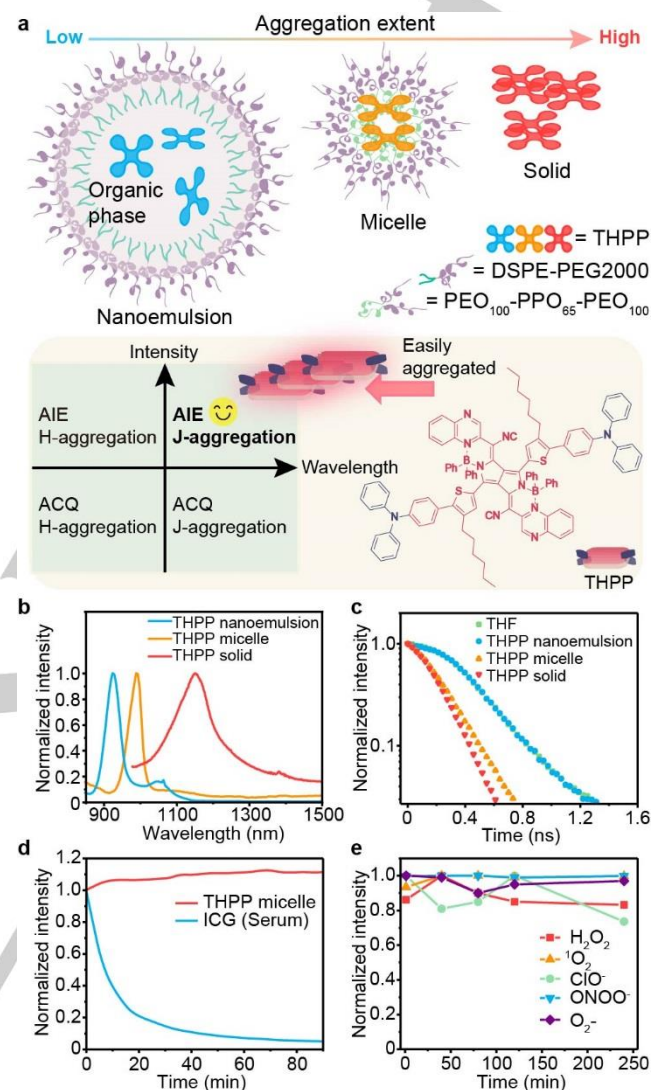


**Figure 2.** a) Scheme for the nanoemulsion, micelle and solid of **THPP** represent different aggregation extent respectively (above) and quadrant diagram for the special AIE and J-aggregation feature of **THPP** (below) b) Normalized emission spectra of F127 micelle, nanoemulsion, and solid of **THPP**. c) Lifetime of organic solution, nanoemulsion, micelle, and solid of **THPP**. d) Normalized fluorescence intensity of **THPP** and ICG (incubated with serum) illuminated with 808 nm pump light (femtosecond laser). e) Normalized fluorescence intensity of **THPP** micelle treated with different ROS and RNS. For b,d&e, the fluorescent emission were recorded at 1000 nm.

To endow **THPP** water solubility for bioimaging, amphiphilic polymers (F127, PEO<sub>100</sub>-PPO<sub>65</sub>-PEO<sub>100</sub>) were used as a shell (Figure 2a), which showed the hydrodynamic size and average diameter of 5.4 nm (DLS, Figure S2) and 4.9 nm (TEM, Figure S3), respectively. Compared to that in the DCM or THF solution, the emission wavelength of the **THPP** micelle shifted to  $\sim 1000 \text{ nm}$  and the intensity showed 10 folds enhancement ( $\epsilon\Phi_f = 1440 \text{ M}^{-1} \text{ cm}^{-1}$ ). Both the enhanced intensity and bathochromic shifted

## COMMUNICATION

wavelength signify the similar aggregated state with that in the THF/H<sub>2</sub>O mixed solution (Figure 1e) and the absolute brightness ( $\epsilon\Phi$ ) in aggregated states are much higher than reported dyes (Table S1 and S2). To further investigate the influence caused by aggregation extent, it is necessary to explore the feature of **THPP** in solid state (aggregated limit). The maximum emission wavelength of solid **THPP** substantially shifted to 1152 nm (Figure 2b). To the best of our knowledge, it is a rather long wavelength of organic solid fluorescence reported by now,<sup>[16]</sup> and the signal can still be captured even by using a 1500 nm long-pass filter (Figure S4). Furthermore, the lifetime of **THPP** in solid state ( $\tau = 275$  ps) is comparable to that of **THPP** micelle ( $\tau = 282$  ps), suggesting the similar aggregated state in these two forms (Figure 2c). The delicate variations between the lifetimes should be ascribed to the different aggregation extent.<sup>[17]</sup> All these findings confirmed the special J-aggregated AIE feature of **THPP** (Figure 2a and S5, quadrantal diagram).

**Table 1.** Photophysical properties of **THPP** in different states.

State	$\epsilon$ (M <sup>-1</sup> cm <sup>-1</sup> )	$\lambda_{abs}$ (nm)	$\lambda_{em}$ (nm)	$\Phi$ (%)[a]	$\epsilon\Phi$ (M <sup>-1</sup> cm <sup>-1</sup> )
DCM	2.0×10 <sup>5</sup>	900	920	0.02	40
THF	2.0×10 <sup>5</sup>	900	932	0.07	140
n-hexane	2.0×10 <sup>5</sup>	900	920	3.0	6000
Lipid Paraffin	2.0×10 <sup>5</sup>	900	920	3.0	6000
Glycerid	2.1×10 <sup>5</sup>	900	920	3.2	6720
THF:H <sub>2</sub> O=1:9[b]	2.2×10 <sup>5</sup>	980	1006	>3.5	>7700
F127 micelle	2.4×10 <sup>5</sup>	970	990	0.6	1440
Solid	NA	NA	1152	NA	NA

[a] The quantum yield of all the states are confirmed by IR26 ( $\Phi = 0.05\%$ ). [b] The refractive indices of water ( $n_s = 1.333$ ) is adopted approximately equal to the mixed solution (THF:H<sub>2</sub>O = 1:9).

It should be noted that the molecular microenvironment of **THPP** plays a key role on the aggregation state of **THPP**. We chose phospholipid (DSPE-PEG2000) to incorporate **THPP** in an apolar organic phase (glyceride) as a control (Figure 2a), which yielded **THPP** nanoemulsion. Unlike the **THPP** micelle, **THPP** nanoemulsion exhibits much larger size ( $d = 42.6$  nm, Figure S2) with a maximum emission peak at 920 nm similar to organic solution. In addition, the lifetime of **THPP** nanoemulsion ( $\tau = 593$  ps) was also similar to that in THF solution ( $\tau = 561$  ps, Figure 2c), indicating monodispersed **THPP** in the nanoemulsion. However, the monodispersed **THPP** nanoemulsion cannot afford a longer wavelength induced by J-aggregation just like **THPP** micelle. Benefiting from the rigid planar structure, **THPP** micelle not only exhibits much higher photostability under a pump laser at a super high power density (16 kW cm<sup>-2</sup>, 80 MHz, pulse width = 10 fs) than that of ICG in serum (Figure 2d and S2), but also shows high chemical stability in various reactive oxygen/nitrogen species (ROS/RNS) (Figure 2e and Table S3). It is worth to mention that **THPP** micelle exhibits over 8 times enhancement of intensity

(>1200 nm) than that of optimized ICG/protein complex (Figure S6).

The *in vitro* tissue penetration depth was examined by capillary filled with **THPP** micelle, with 1% intralipid as mimic tissues (Figure S7). To keep the experiment conditions consistent with that for further *in vivo* imaging, the power density was kept at 50 mW cm<sup>-2</sup>, and the concentration (20  $\mu$ M, dispersed in serum) was adopted at a fifth to a tenth of the concentration for actual tail vein injection (100-200  $\mu$ M) into a mouse to simulate the dilution process in blood.<sup>[18]</sup> As can be seen in Figure S7, the visibility of the capillary signals deteriorated as the tissue depth increased from 0 to 7.5 mm, together with the FWHM increased from 0.9 mm to 4.5 mm. Under the above situations, this 'valid tissue penetration depth' was estimated to be about 6 mm (with SNR above 5), suggesting the potential use of **THPP** micelle for high contrast imaging in deep tissue (Figure S7, Table S4).

Based on the above merits, **THPP** micelle encouraged us for high resolution *in vivo* bioimaging. Before these, the potential cytotoxicity of **THPP** micelle was evaluated, which showed a good biocompatibility (Figure S9). We first compared cerebral vasculature of mice by using Food and Drug Administration (FDA) approved ICG as a control in both NIR-I (850 - 950 nm) and NIR-II (> 1200 nm) window (Figure 3a, S8). The main cerebral vessels lighted by **THPP** micelle are much clearer than that of ICG in NIR-II window, with a 3 times higher brightness and a sharper FWHM at 0.5 mm compared with FWHM = 0.7 mm for imaging using ICG). When imaging in the NIR-I window, blurred images were obtained and cerebral vessels could hardly be resolved due to the enhanced scattering effect and tissue autofluorescence background (Figure 3a). Similar improvement on spatial resolution were also confirmed by imaging of body vasculatures using **THPP** micelles (Figure S8).

In addition to the high spatial resolution, **THPP** micelle can also be adopted for dynamic imaging with high temporal resolution. To show this advantage, we performed sequential imaging of the deep organs. At 3 s post injection (p.i.) of **THPP** micelles via tail (100  $\mu$ M, 200  $\mu$ L), the lung lobes were firstly highlighted from the dorsal view (Figure 3b, c and Supplementary Video 1). Then NIR-II fluorescence signals began to show in aorta at about 0.5 second later, followed by the appearance of spine and kidneys (at about 5.3 s p.i.). These results indicating **THPP** micelle first pumped by the heart into the pulmonary artery to the lungs and then flowed through the aorta to the systemic arterial and finally to other organs such as spine and kidneys. All the processes above were consistent with the pulmonary circulation and systemic circulation as reported (Figure 3d, S10).<sup>[19]</sup> When further increase the imaging rate (34.5 FPS), physiological activities such as cardiac cycle can be directly visualized and monitored using **THPP** micelles, which cannot be easily done through optical imaging before. At the mild power density (50 mW cm<sup>-2</sup>) and short exposure time (50 ms), a typical cone shaped heart was highlighted by **THPP** micelles with alternatively diastole and systole states based on the contrast of the NIR-II fluorescence signals. Although the heart was rapidly fused with lungs due to pulmonary circulation, the variation of signals indicating heartbeat could still be easily resolved overtime (Supplementary Video 2). The recorded heartbeat rate of 414 beats min<sup>-1</sup> (Figure 3f and h) is in line with previous report.<sup>[20]</sup> The direct monitoring of heartbeat may show a much more accurate

## COMMUNICATION

way than other indirect vascular or organ vibration. Besides, the high imaging rate also ensures integrity of the data without any data loss as compared to that of low imaging rate at 8.6 FPS, which gives the heartbeat at only 108 beats  $\text{min}^{-1}$  (Figure 3g). As a control, heartbeat of mice was also monitored by ICG. However, the outline of the heart can hardly be profiled by a 5 times lower

brightness and 8 times lower in SNR at the same power density and exposure time (Figure 3h and i). Besides, owing to the fast coordination with protein in the blood, ICG would be soon ( $< 10$  s) accumulated in the liver (yellow circle, Figure 3e), together with signal decreasing from other organs and vasculatures (Supplementary video 2).

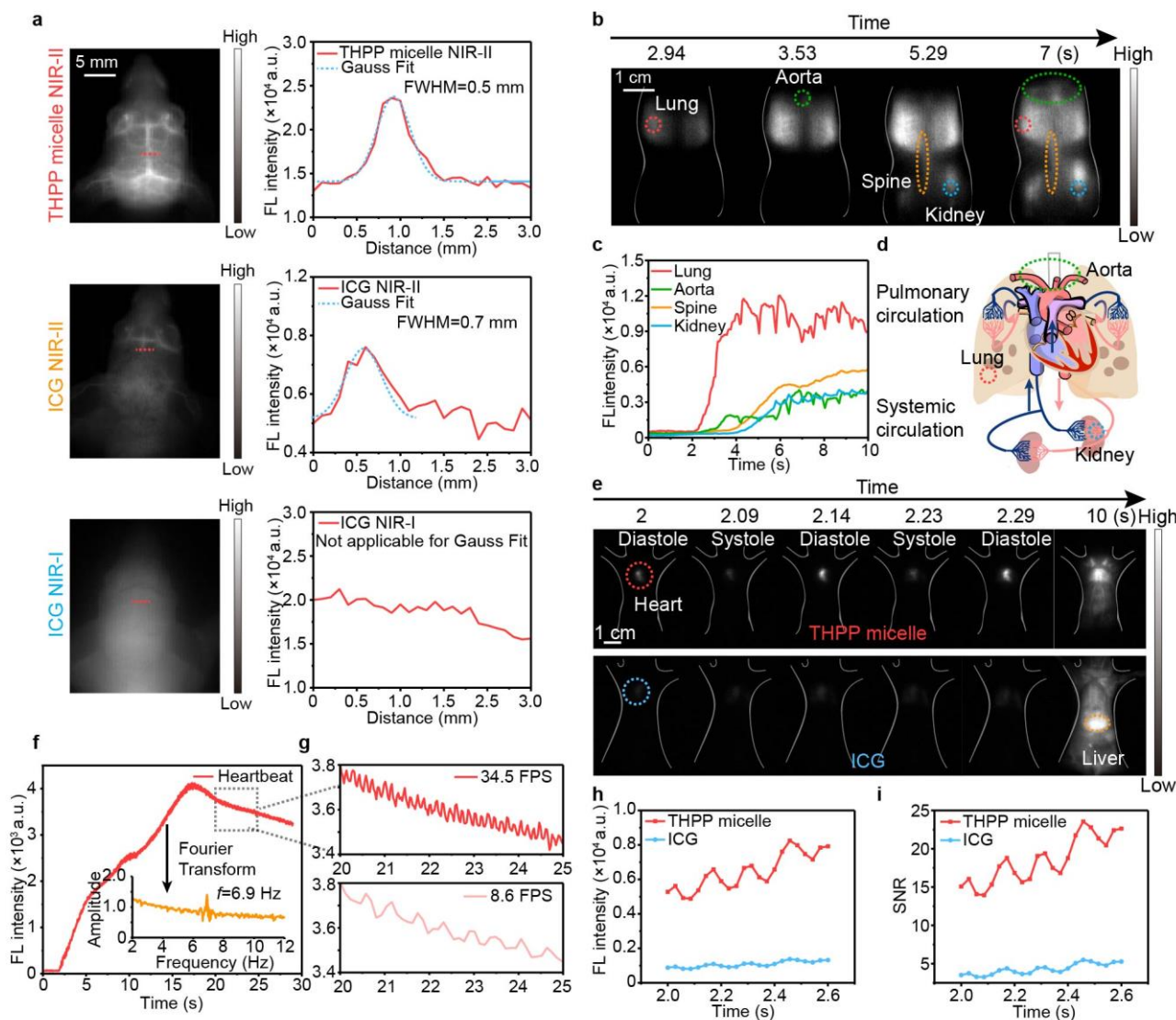


**Figure 3.** a) Cerebral vasculature imaging and fluorescence intensity profiles from the dashed red line of **THPP** micelles, ICG in the NIR-I (850 nm-950 nm) and NIR-II window ( $> 1200$  nm). b) NIR-II imaging at 17 FPS from dorsal view of a nude mouse over time (tail vein injection of 100  $\mu\text{M}$ , 200  $\mu\text{L}$  **THPP** micelles). c) Fluorescence intensity profiles of lungs, aorta, kidney and spine (dashed circles). d) Schematic illustration for pulmonary circulation and systemic circulation. e) NIR-II imaging at 34.5 FPS from ventral view of anesthetized nude mouse (exposure time = 20 ms) after tail vein injection of **THPP** micelles (200  $\mu\text{M}$ , 200  $\mu\text{L}$ ) and ICG (50  $\mu\text{M}$ , 200  $\mu\text{L}$ ). f) Fluorescence intensity of the heart (red dashed circles in e) versus time. Inset shows a heartbeat frequency of 6.9 Hz by fast Fourier transformation. g) Fluorescence intensity of the heart extracted at a low frame rate (8.6 FPS). h) Average fluorescence intensity and i) SNRs of the heart using **THPP** micelles (red dashed circles in e) and ICG (blue dashed circles in e) versus time. **THPP** was excited by 980 nm laser at power density of 50  $\text{mW cm}^{-2}$ , with a 1200 nm long-pass filter. ICG was excited at 808 nm laser at power density of 50  $\text{mW cm}^{-2}$ , with a 1200 nm long-pass filter. The exposure time = 50 ms.

## COMMUNICATION

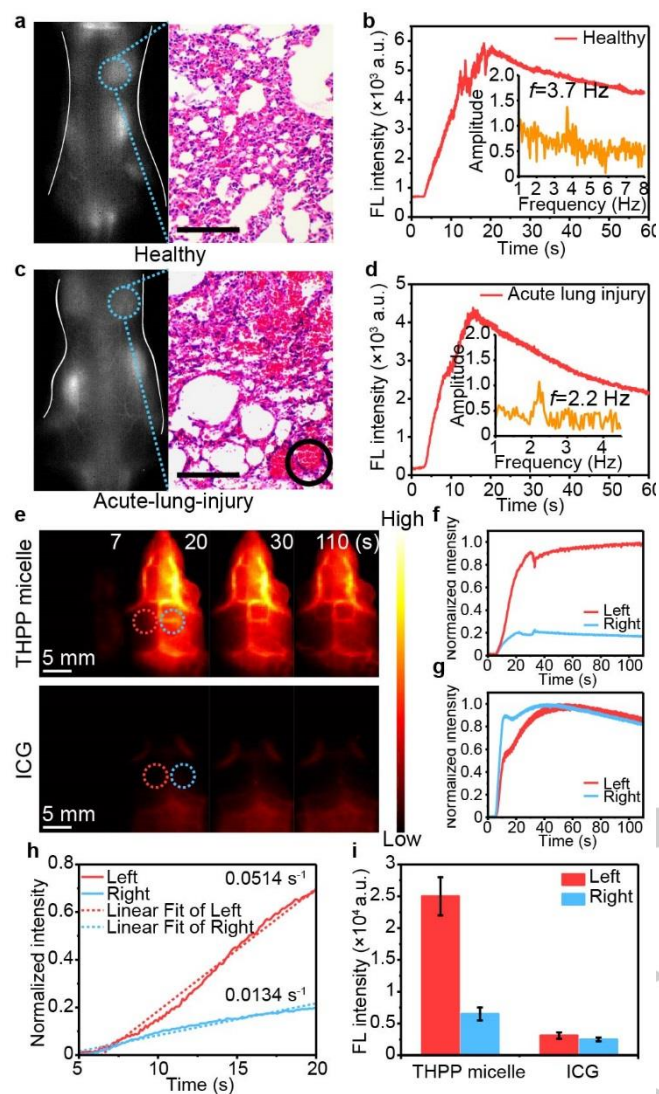


**Figure 4.** Dorsal view of a) Healthy group in conscious state without any treatments and d) lipopolysaccharide induced acute-lung-injury group (administration of 10 ng lipopolysaccharide) in conscious state, together with histopathological examination of lung tissue sections stained by Hematoxylin and eosin (H&E, original magnification,  $\times 200$ , scale bar = 100  $\mu\text{m}$ ). Fluorescence intensity of the b) healthy group and e) Acute-lung-injury group profiles the region of lungs from the dorsal view, and the inset is frequency analyzed from the variation after Fourier transform. The respiratory rate of c) healthy group and f) Acute-lung-injury group filtered by 0.5 Hz high-pass filter. g) Cerebral vasculature imaging of mice with carotid arterial thrombosis to the left hemisphere versus time, imaged using **THPP** micelles (200  $\mu\text{M}$ , 200  $\mu\text{L}$ ) and ICG (50  $\mu\text{M}$ , 200  $\mu\text{L}$ ). h) Normalized NIR-II signal in the left (red) and right (blue) cerebral hemispheres extracted from g using **THPP** micelles. i) Normalized NIR-II signal in the left (red) and right (blue) cerebral hemispheres extracted from g using ICG. j) Comparison of the absolute intensity in the dashed red (blue) line between **THPP** micelle and ICG. **THPP** was excited by 980 nm laser at power density of 50  $\text{mW cm}^{-2}$ , 1200 nm LP. ICG was excited at 808 nm laser at power density of 50  $\text{mW cm}^{-2}$ , 1200 nm LP. The exposure time = 50 ms.

The **THPP** micelles were further adopted for acute-lung-injury to evaluate the respiratory rate, and tracing the collateral circulation process of mice. In the acute-lung-injury model with the

pulmonary dysfunction (Figure 4a and c, Supplementary Video 3), the respiratory rate was detected to be 126 breaths  $\text{min}^{-1}$ , which was 76% times lower than that for the healthy mice (222 breaths  $\text{min}^{-1}$ ) extracted from the signals of lung vibration (Figure 4b and d). As a control, the respiratory rate of deeply anaesthetized mice was also recorded (78 breaths  $\text{min}^{-1}$ , Figure S11).

The collateral circulation is a self-protective mechanism induced by the vascular thrombosis, which plays important role in restoring blood supply to the damaged area. Immediately after tail-vein injection of **THPP** micelles into a mice with  $\text{FeCl}_3$  induced carotid arterial thrombosis as a model for stroke to the left cerebral hemisphere, we performed dynamic brain imaging (17 FPS). An NIR-II signal arising from the lateral sulcus on right side of the cerebrum within 20s post injection (Figure 4g). However, the left hemisphere exhibited a marked delay of blood flow. The dynamic NIR-II imaging of **THPP** micelles provided possibilities to quantify the cerebral vasculature perfusion through the average intensity of selected areas (Figure 4h, supplementary video 4). The linearly rising fluorescence signals in left hemisphere was 0.0134  $\text{s}^{-1}$ , however the right hemisphere was 0.0514  $\text{s}^{-1}$ , which showed a remarkable difference in blood perfusion (Figure 4i). Corresponding to the decrease of fluorescence signals at the right side at 20 s (Figure 4h), the left side showed a delayed increase and then dropped at 30 s, which suggested a continuous blood supply from the right part to the left part through the terminal collateral circulation. In addition, the opposite fluorescence signals changes in the left and right hemisphere after 40 s also confirmed the collateral circulation in the terminal blood vessels. For comparison, we also performed the same experiment using ICG. As shown in Figure 4j, the variations of cerebral vessels in left and right hemisphere are hard to differentiate, let alone the analysis of collateral circulation, which is largely owing to the low brightness of ICG in NIR-II window (Figure 4k).

In summary, a NIR-II J-aggregated AIE molecule **THPP** was designed and synthesized with high MEC and absorptivity, showing a strong brightness ( $\epsilon\Phi_f > 7700 \text{ M}^{-1}\text{cm}^{-1}$ ) in aqueous, which is highly boosted by the typical reduction of thermal deactivation.<sup>[21]</sup> Owing to the rigid planar structure, **THPP** shows much higher photostability and chemical stability compared to that of ICG/protein combinations, which is commonly used and FDA approved in NIR bioimaging. Taking advantages of the brightness of **THPP** micelle and the long emission wavelength in the NIR-II region, the deeply located viscera could be easily shown, offering a contact-free and effectively optical way to reveal the pulmonary circulation and systemic circulation in living mice. With the help of **THPP**, we could easily distinguish the acute-lung-injury mice and healthy mice by dynamically monitoring the respiratory. Furthermore, the collateral circulation process could be clearly monitored with a high frame rate. Future work will focus on the modification of the donor structure to adjust the band gap and eventually enlarge the Stokes shift, meanwhile the balance between the MEC and QY is also a critical point for novel chromophores (e.g. combination of twisted and planar structure).<sup>[22]</sup> Combing merits of AIE and J-aggregation properties, **THPP** will be uniquely positioned in the NIR-II bioimaging applications.

## COMMUNICATION

## Acknowledgements

This work was supported by the National Key R&D Program of China (2017YFA0207303), National Natural Science Foundation of China (NSFC, 21725502, 51961145403, 21904023), and Research Program of Science and Technology Commission of Shanghai Municipality (17JC1400100, 19490713100, 20490710600).

**Keywords:** NIR-II • J-aggregated • AIE • dibodipy • bioimaging

- [1] a) H. Yao, Y. Zhang, F. Xiao, Z. Xia, J. Rao, *Angew. Chem. Int. Ed. Engl.* **2007**, *46*, 4346-4349; b) S. Lee, J. Xie, X. Chen, *Chem. Rev.* **2010**, *110*, 3087-3111; c) H. Kobayashi, M. Ogawa, R. Alford, P. L. Choyke, Y. Urano, *Chem. Rev.* **2010**, *110*, 2620-2640; d) J. Qian, D. Wang, F. H. Cai, W. Xi, L. Peng, Z. F. Zhu, H. He, M. L. Hu, S. He, *Angew. Chem.* **2012**, *124*, 10722-10727; e) Y. Sun, X. Ma, K. Cheng, B. Wu, J. Duan, H. Chen, L. Bu, R. Zhang, X. Hu, Z. Deng, L. Xing, X. Hong, Z. Cheng, *Angew. Chem. Int. Ed. Engl.* **2015**, *54*, 5981-5984; f) Q. Miao, C. Xie, X. Zhen, Y. Lyu, H. Duan, X. Liu, J. V. Jokerst, K. Pu, *Nat. Biotechnol.* **2017**, *35*, 1102-1110; g) Y. Tang, Y. Li, X. Hu, H. Zhao, Y. Ji, L. Chen, W. Hu, W. Zhang, X. Li, X. Lu, W. Huang, Q. Fan, *Adv. Mater.* **2018**, *30*, e1801140; h) L. Wang, W. Du, Z. Hu, K. Uvdal, L. Li, W. Huang, *Angew. Chem. Int. Ed. Engl.* **2019**, *58*, 14026-14043; i) S. Ling, X. Yang, C. Li, Y. Zhang, H. Yang, G. Chen, Q. Wang, *Angew. Chem. Int. Ed.* **2020**, *59*, 7219-7223.
- [2] a) H. Shi, X. He, K. Wang, X. Wu, X. Ye, Q. Guo, W. Tan, Z. Qing, X. Yang, B. Zhou, *Proc. Natl. Acad. Sci. U. S. A.* **2011**, *108*, 3900-3905; b) T. L. Doane, C. Burda, *Chem. Soc. Rev.* **2012**, *41*, 2885-2911; c) Y. M. Yang, Q. Shao, R. R. Deng, C. Wang, X. Teng, K. Cheng, Z. Cheng, L. Huang, Z. Liu, X. G. Liu, B. G. Xing, *Angew. Chem. Int. Ed.* **2012**, *51*, 3125-3129; d) A. J. Shuhendler, K. Pu, L. Cui, J. P. Uetrecht, J. Rao, *Nat. Biotechnol.* **2014**, *32*, 373-380; e) Y. Min, J. Li, F. Liu, E. K. Yeow, B. Xing, *Angew. Chem.* **2014**, *126*, 1030-1034.
- [3] a) Q. T. Nguyen, R. Y. Tsien, *Nat. Rev. Cancer* **2013**, *13*, 653-662; b) P. Wang, Y. Fan, L. Lu, L. Liu, L. Fan, M. Zhao, Y. Xie, C. Xu, F. Zhang, *Nat. Commun.* **2018**, *9*, 2898; c) Y. Sun, F. Ding, Z. Zhou, C. Li, M. Pu, Y. Xu, Y. Zhan, X. Lu, H. Li, G. Yang, Y. Sun, P. J. Stang, *Proc. Natl. Acad. Sci. U. S. A.* **2019**, *116*, 1968-1973; d) R. Tian, H. Ma, S. Zhu, J. Lau, R. Ma, Y. Liu, L. Lin, S. Chandra, S. Wang, X. Zhu, H. Deng, G. Niu, M. Zhang, A. L. Antaris, K. S. Hettie, B. Yang, Y. Liang, X. Chen, *Adv. Mater.* **2020**, *32*, e1907365.
- [4] a) K. Welsher, Z. Liu, S. P. Sherlock, J. T. Robinson, Z. Chen, D. Daranciang, H. Dai, *Nat. Nanotech.* **2009**, *4*, 773-780; b) K. Pu, A. J. Shuhendler, J. V. Jokerst, J. Mei, S. S. Gambhir, Z. Bao, J. Rao, *Nat. Nanotech.* **2014**, *9*, 233-239; c) Y. Fan, P. Wang, Y. Lu, R. Wang, L. Zhou, X. Zheng, X. Li, J. A. Piper, F. Zhang, *Nat. Nanotech.* **2018**, *13*, 941-946; d) H. Zhang, Y. Fan, P. Pei, C. Sun, L. Lu, F. Zhang, *Angew. Chem.* **2019**, *131*, 10259-10263.
- [5] a) G. S. Hong, A. L. Antaris, H. J. Dai, *Nat. Biomed. Eng.* **2017**, *1*, 0010; b) Kenry, Y. Duan, B. Liu, *Adv. Mater.* **2018**, *30*, e1802394; c) F. Ding, Y. Zhan, X. Lu, Y. Sun, *Chem. Sci.* **2018**, *9*, 4370-4380; d) H. Li, M. Tan, X. Wang, F. Li, Y. Zhang, L. Zhao, C. Yang, G. Chen, *J. Am. Chem. Soc.* **2020**, *142*, 2023-2030.
- [6] a) B. Cool, B. Zinker, W. Chiou, L. Kifle, N. Cao, M. Perham, R. Dickinson, A. Adler, G. Gagne, R. Iyengar, G. Zhao, K. Marsh, P. Kym, P. Jung, H. S. Camp, E. Frevert, *Cell Metab.* **2006**, *3*, 403-416; b) P. P. Hsu, D. M. Sabatini, *Cell* **2008**, *134*, 703-707.
- [7] a) S. He, J. Song, J. Qu, Z. Cheng, *Chem. Soc. Rev.* **2018**, *47*, 4258-4278; b) F. Wang, H. Wan, Z. Ma, Y. Zhong, Q. Sun, Y. Tian, L. Qu, H. Du, M. Zhang, L. Li, H. Ma, J. Luo, Y. Liang, W. J. Li, G. Hong, L. Liu, H. Dai, *Nat. Methods* **2019**, *16*, 545-552; c) L. Bai, P. Sun, Y. Liu, H. Zhang, W. Hu, W. Zhang, Z. Liu, Q. Fan, L. Li, W. Huang, *Chem. Commun.* **2019**, *55*, 10920-10923; d) F. Xiao, L. Lin, Z. Chao, C. Shao, Z. Chen, Z. Wei, J. Lu, Y. Huang, L. Li, Q. Liu, Y. Liang, T. leilei, *Angew. Chem.* **2020**, *132*, 9789-9797.
- [8] a) A. L. Antaris, H. Chen, K. Cheng, Y. Sun, G. Hong, C. Qu, S. Diao, Z. Deng, X. Hu, B. Zhang, X. Zhang, O. K. Yaghi, Z. R. Alamparambil, X. Hong, Z. Cheng, H. Dai, *Nat. Mater.* **2016**, *15*, 235-242; b) E. D. Cosco, J. R. Caram, O. T. Bruns, D. Franke, R. A. Day, E. P. Farr, M. G. Bawendi, E. M. Sletten, *Angew. Chem. Int. Ed. Engl.* **2017**, *56*, 13126-13129; c) B. Li, L. Lu, M. Zhao, Z. Lei, F. Zhang, *Angew. Chem. Int. Ed. Engl.* **2018**, *57*, 7483-7487; d) J. A. Carr, D. Franke, J. R. Caram, C. F. Perkinson, M. Saif, V. Askoxylakis, M. Datta, D. Fukumura, R. K. Jain, M. G. Bawendi, O. T. Bruns, *Proc. Natl. Acad. Sci. U. S. A.* **2018**, *115*, 4465-4470; e) J. Huang, C. Xie, X. Zhang, Y. Jiang, J. Li, Q. Fan, K. Pu, *Angew. Chem. Int. Ed.* **2019**, *58*, 15120-15127; f) B. Li, M. Zhao, L. Feng, C. Dou, S. Ding, G. Zhou, L. Lu, H. Zhang, F. Chen, X. Li, G. Li, S. Zhao, C. Jiang, Y. Wang, D. Zhao, Y. Cheng, F. Zhang, *Nat. Commun.* **2020**, *11*, 3102; g) Y. Yang, S. Wang, L. Lu, Q. Zhang, P. Yu, Y. Fan, F. Zhang, *Angew. Chem. Int. Ed.* **2020**.
- [9] a) Z. Lei, C. Sun, P. Pei, S. Wang, D. Li, X. Zhang, F. Zhang, *Angew. Chem. Int. Ed.* **2019**, *58*, 8166-8171; b) S. Wang, Y. Fan, D. Li, C. Sun, Z. Lei, L. Lu, T. Wang, F. Zhang, *Nat. Commun.* **2019**, *10*, 1058.
- [10] a) H. B. Shi, R. T. K. Kwok, J. Z. Liu, B. G. Xing, B. Z. Tang, B. Liu, J. Am. Chem. Soc. **2012**, *134*, 17972-17981; b) D. Ding, K. Li, B. Liu, B. Z. Tang, *Acc. Chem. Res.* **2013**, *46*, 2441-2453; c) C. W. Leung, Y. Hong, S. Chen, E. Zhao, J. W. Lam, B. Z. Tang, *J. Am. Chem. Soc.* **2013**, *135*, 62-65; d) J. Qian, B. Z. Tang, *Chem* **2017**, *3*, 56-91; e) H. T. Feng, Y. X. Yuan, J. B. Xiong, Y. S. Zheng, B. Z. Tang, *Chem. Soc. Rev.* **2018**, *47*, 7452-7476; f) F. Hu, D. Mao, X. Cai, W. Wu, D. Kong, B. Liu, *Angew. Chem.* **2018**, *130*, 10339-10343; g) S. Liu, X. Zhou, H. Zhang, H. Ou, J. W. Y. Lam, Y. Liu, L. Shi, D. Ding, B. Z. Tang, *J. Am. Chem. Soc.* **2019**, *141*, 5359-5368; h) H. Chen, S. Li, M. Wu, Z. Huang, C. S. Lee, B. Liu, *Angew. Chem. Int. Ed.* **2020**, *59*, 632-636; i) W. Xu, D. Wang, B. Z. Tang, *Angew. Chem.* **2020**; j) S. Suzuki, S. Sasaki, A. S. Sairi, R. Iwai, B. Z. Tang, G. i. Konishi, *Angew. Chem.* **2020**, *132*, 9940-9951; k) W. Xu, M. M. Lee, J. J. Nie, Z. Zhang, R. T. Kwok, J. W. Lam, F. J. Xu, D. Wang, B. Z. Tang, *Angew. Chem. Int. Ed.* **2020**, *59*, 9610-9616.
- [11] Y. Hong, J. W. Lam, B. Z. Tang, *Chem. Soc. Rev.* **2011**, *40*, 5361-5388.
- [12] S. Wang, J. Liu, C. C. Goh, L. G. Ng, B. Liu, *Adv. Mater.* **2019**, *31*, e1904447.
- [13] a) K. Cai, J. Xie, D. Zhao, *J. Am. Chem. Soc.* **2014**, *136*, 28-31; b) P. Sun, Q. Wu, X. Sun, H. Miao, W. Deng, W. Zhang, Q. Fan, W. Huang, *Chem. Commun.* **2018**, *54*, 13395-13398; c) C. Sun, B. Li, M. Zhao, S. Wang, Z. Lei, L. Lu, H. Zhang, L. Feng, C. Dou, D. Yin, H. Xu, Y. Cheng, F. Zhang, *J. Am. Chem. Soc.* **2019**, *141*, 19221-19225; d) M. H. Cheng, K. M. Harmatys, D. M. Charron, J. Chen, G. Zheng, *Angew. Chem.* **2019**, *131*, 13528-13533.
- [14] a) W. Rettig, *Angew. Chem. Int. Ed.* **1986**, *25*, 971-988; b) C. Wang, Q. Qiao, W. Chi, J. Chen, W. Liu, D. Tan, S. McKechnie, D. Lyu, X. F. Jiang, W. Zhou, N. Xu, Q. Zhang, Z. Xu, X. Liu, *Angew. Chem. Int. Ed. Engl.* **2020**, *59*, 10160-10172.
- [15] F. Würthner, T. E. Kaiser, C. R. Saha - Möller, *Angew. Chem. Int. Ed.* **2011**, *50*, 3376-3410.
- [16] a) L. Yao, S. Zhang, R. Wang, W. Li, F. Shen, B. Yang, Y. Ma, *Angew. Chem. Int. Ed.* **2014**, *53*, 2119-2123; b) P. Data, P. Pander, M. Okazaki, Y. Takeda, S. Minakata, A. P. Monkman, *Angew. Chem.* **2016**, *128*, 5833-5838; c) K. T. Ly, R. W. Chen-Cheng, H. W. Lin, Y. J. Shiau, S. H. Liu, P. T. Chou, C. S. Tsao, Y. C. Huang, Y. Chi, *Nat. Photon.* **2017**, *11*, 63-68.
- [17] a) K. Kernitz, K. Yoshihara, T. Tani, *J. Phys. Chem.* **1990**, *94*, 3099-3104; b) T. E. Kaiser, H. Wang, V. Stepanenko, F. Würthner, *Angew. Chem. Int. Ed. Engl.* **2007**, *46*, 5541-5544.
- [18] H. He, J. Zhang, Y. Xie, Y. Lu, J. Qi, E. Ahmad, X. Dong, W. Zhao, W. Wu, *Mol. Pharmaceut.* **2016**, *13*, 4013-4019.
- [19] J. A. Beckman, *Circulation* **2002**, *106*, 2170-2172.
- [20] D. Ho, X. Zhao, S. Gao, C. Hong, D. E. Vatner, S. F. Vatner, *Curr. Protoc. mouse Biol.* **2011**, *1*, 123-139.
- [21] a) J. Qi, C. Chen, X. Y. Zhang, X. L. Hu, S. L. Ji, R. T. K. Kwok, J. W. Y. Lam, D. Ding, B. Z. Tang, *Nat. Commun.* **2018**, *9*; b) C. Chen, X. Ni, H. W. Tian, Q. Liu, D. S. Guo, D. Ding, *Angew. Chem. Int. Ed.* **2020**, *59*, 10008-10012.
- [22] a) X. Ni, X. Zhang, X. Duan, H.-L. Zheng, X.-S. Xue, D. J. N. I. Ding, **2018**, *19*, 318-330; b) S. Liu, H. Ou, Y. Li, H. Zhang, J. Liu, X. Lu, R. T. K. Kwok, J. W. Y. Lam, D. Ding, B. Z. Tang, *J. Am. Chem. Soc.* **2020**.

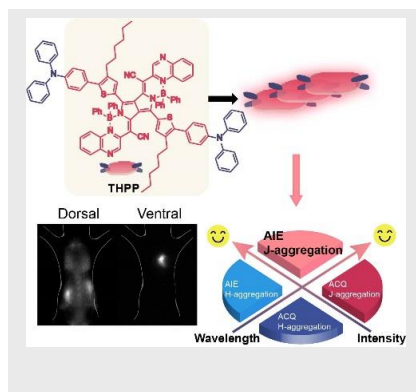
## COMMUNICATION

Entry for the Table of Contents (Please choose one layout)

Layout 1:

## COMMUNICATION

A J-aggregated AIE dibodipy **THPP** was synthesized with enhanced fluorescence intensity in the NIR-II window for dynamic *in vivo* imaging.



Qisong Zhang, Peng Yu, Yong Fan\*,  
Caixia Sun, Haisheng He, Xuan Liu,  
Lingfei Lu, Mengyao Zhao, Fan Zhang\*

Page No. – Page No.

**Bright and Stable NIR-II J-aggregated  
AIE Dibodipy for Dynamic *in vivo*  
Bioimaging**